Taylor & Francis
Taylor & Francis Group

Journal of Earthquake Engineering

ISSN: 1363-2469 (Print) 1559-808X (Online) Journal homepage: http://www.tandfonline.com/loi/ueqe20

On the Earthquake-Source Numerical Implementation in the Seismic Wave Equation

José M. Carcione, Fabio Cavallini, Davide Gei & Marco A. B. Botelho

To cite this article: José M. Carcione, Fabio Cavallini, Davide Gei & Marco A. B. Botelho (2015) On the Earthquake-Source Numerical Implementation in the Seismic Wave Equation, Journal of Earthquake Engineering, 19:1, 48-59, DOI: 10.1080/13632469.2014.966178

To link to this article: http://dx.doi.org/10.1080/13632469.2014.966178

Accepted online: 06 Oct 2014.

Journal of Earthquake Engineering, 19:48–59, 2015

ISSN: 1363-2469 print / 1559-808X online
DOI: 10.1080/13632469.2014.966178

Taylor & Francis
Taylor & Francis Group

On the Earthquake-Source Numerical Implementation in the Seismic Wave Equation

JOSÉ M. CARCIONE[1], FABIO CAVALLINI[1], DAVIDE GEI[1], and MARCO A. B. BOTELHO[2]

[1]Istituto Nazionale di Oceanografia e di Geofisica Sperimentale (OGS), Trieste, Italy
[2]Instituto de Geociências, Campus Universitário de Ondina, Universidade Federal da Bahia, Salvador-BA, Brasil

We present a detailed approach to implement a moment-tensor point source to compute displacements, particle velocities and accelerations using direct grid methods. Here, the wave modeling algorithm is based on pseudospectral methods to compute the partial derivatives. A comparison to the analytical solution in the 3D acoustic case verifies the discrete implementation of the source in the mesh. Then, the more general 3D elastic case is illustrated and simulations, with and without free surface, are performed that can be used as a reference solution for other grid methods.

Keywords Earthquake; Source; Modeling; Moment-Tensor; Direct Grid Method

1. Introduction

The correct source modeling in direct grid methods is essential in earthquake seismology to compute ground displacements, particle-velocities and accelerations as an aid in the generation of reliable seismic hazard maps. The approach is partially outlined in the literature but not fully detailed and verified (e.g., Graves, 1996; Pitarka, 1999). In most of the cases, there is not even the complete information (e.g., wave shape, frequency) to reproduce the results, yet being this aspect of earthquake modeling essential. We show in this work the details of the source implementation in a full-wave modeling algorithm, where the spatial derivatives are computed with pseudospectral methods [Carcione, 2007]. The Fourier and Chebyshev methods used here are accurate (negligible numerical dispersion) up to the maximum wavenumber of the mesh that corresponds to a spatial wavelength of two grid points (at maximum grid spacing for the Chebyshev operator). This fact makes these methods very efficient in terms of computer storage (mainly in 3D space) [Carcione *et al.*, 2002]. The comparison to an analytical solution verifies the source implementation. The method applies to finite-difference and finite-element methods (e.g., DGM) and any approach where the space is discretized, such as the boundary element method (BEM). In this method, for instance, the integrands in the source terms of the Green functions can in some cases be calculated in closed form [Tadeu *et al.*, 1999].

The wave equations, recast in the particle velocity-stress formulation, describe 3D P-wave propagation in acoustic media and 3D P- and S-wave propagation in elastic media.

Received 10 September 2013; accepted 11 September 2014.
Address correspondence to José M. Carcione, Istituto Nazionale di Oceanografia e di Geofisica Sperimentale (OGS), Borgo Grotta Gigante 42c, 34010 Sgonico, Trieste, Italy. E-mail: jcarcione@inogs.it

The physical domain is discretized on a mesh and the time solver is a 4th-order Runge-Kutta approximation [Carcione, 2007]. The examples provide a reference solution to verify the source implementation in any direct method algorithm.

2. Acoustic Wave Equation

Let us consider a 3D space described by the coordinates $(x, y, z) = (x_1, x_2, x_3)$. The particle velocity-stress formulation for the acoustic wave equation is (e.g., Carcione, 2007)

$$\begin{aligned} \dot{v}_1 &= \rho^{-1}\partial_1\sigma, \\ \dot{v}_2 &= \rho^{-1}\partial_2\sigma, \\ \dot{v}_3 &= \rho^{-1}\partial_3\sigma, \\ \dot{\sigma} &= \rho c^2(\partial_1 v_1 + \partial_2 v_2 + \partial_3 v_3) + \dot{M}, \end{aligned} \tag{1}$$

where v_i denotes the particle-velocity components, σ is the scalar stress (diagonal component of the stress tensor), M is the source (which corresponds to the moment tensor components in the elastic case), ρ is the density and c is the wave velocity. A dot above a variable indicates time differentiation.

Eq. (1) can be written in terms of the stress as

$$\ddot{\sigma} = c^2\Delta\sigma + \ddot{M}, \tag{2}$$

where Δ is the Laplacian, and we have assumed a homogeneous medium. Let us consider the following source

$$M = M_0\,\delta(x)\,\delta(y)\,\delta(z)\,h(t), \tag{3}$$

where δ denotes Dirac's function, h is the time history and M_0 is the seismic moment. This is usually obtained as $M_0 = A\Delta\sigma_0 s$, where $A\,[\mathrm{m}^2]$ is the area of the fault, $\Delta\sigma_0$ [Pa] is the stress drop, and s [m] is the slip. M_0 has units [Pa m^3] or [J], i.e., units of energy.

The analytical solution of the 3D Green's function equation

$$\ddot{G} = c^2\Delta G + M_0\delta(x)\,\delta(y)\,\delta(z)\,\delta(t), \tag{4}$$

corresponding to (2), is given in Morse and Feshbach (1953, Eq. 7.3.8),

$$G = \frac{M_0}{4\pi c^2 r}\delta\Big(t - \frac{r}{c}\Big). \tag{5}$$

In the 1D case an additional term $\delta(t + r/c)$ has to be included. Since

$$\sigma = G * \ddot{h}, \tag{6}$$

where "*" denotes convolution with respect to time (note the source double time derivative in Eq. (2)), we obtain

$$\sigma = \frac{M_0}{4\pi c^2 r}\ddot{h}\left(t - \frac{r}{c}\right), \tag{7}$$

where

$$r = \sqrt{x^2 + y^2 + z^2}. \tag{8}$$

2.1. Representation of the Source in the Mesh

The discrete representation of a delta function is

$$\delta(x) = \begin{cases} 1/dx & \text{if } x = 0 \\ 0 & \text{otherwise,} \end{cases} \tag{9}$$

where dx is the grid spacing in the x-direction; likewise for $\delta(y)$ and $\delta(z)$. Similarly, a discrete temporal delta is $1/dt$ at the time origin and zero elsewhere, where dt is the time step of the time solver.

Therefore, the discrete source is

$$M = M_0\delta(x)\,\delta(y)\,\delta(z)\,h(t) = M_0\frac{1}{dx}\frac{1}{dy}\frac{1}{dz}h(t) = \frac{M_0}{V}h(t), \tag{10}$$

where $V = dx\,dy\,dz$ is the volume of the cell, in agreement with the source implementation in Pitarka [1999]. In variable-grid algorithms, V is the volume of a finite-difference cell as indicated by Pitarka [1999].

The time history h is dimensionless and must satisfy [Dahlen and Tromp, 1998]

$$\int_0^\infty |\dot{h}|\,dt = 1. \tag{11}$$

2.2. The Time History of the Source

A set of Ricker time histories can be generated with the function $2g_0 = \exp(-a^2)$, where a depends on the peak frequency of the spectrum f_p (see below) [Sheriff, 2002]. If $g_v = d^v g_0/dt^v$,

$$\begin{aligned} 2g_0 &= \omega_p^0 \exp(-a^2), \quad a = \pi t f_p, \qquad \omega_p = 2\pi f_p, \\ 2g_1 &= \omega_p^1(-a)\exp(-a^2), \\ 2g_2 &= \omega_p^2(a^2 - 1/2)\exp(-a^2), \\ 2g_3 &= \omega_p^3(-a^3 + 3a/2)\exp(-a^2), \\ 2g_4 &= \omega_p^4(a^4 - 3a^2 + 3/4)\exp(-a^2), \end{aligned} \tag{12}$$

Figure 1 shows g_0, g_1, g_2 and g_3 as a function of time for $f_p = 1$ Hz and delayed by $1.4/f_p$.

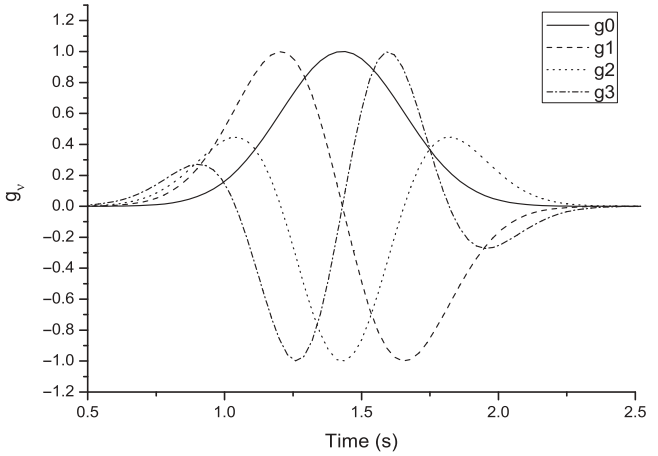

FIGURE 1 Normalized time histories g_v.

Let us assume

$$\begin{aligned} 2h(t) &= 2g_0(t-t_s) = \exp\left(-b^2\right), \qquad b = \pi(t-t_s)f_p, \\ 2\dot{h}(t) &= 2g_1(t-t_s) = \omega_p(-b)\exp\left(-b^2\right), \\ 2\ddot{h}(t) &= 2g_2(t-t_s) = \omega_p^2\left(b^2-1/2\right)\exp\left(-b^2\right), \\ 2\dddot{h}(t) &= 2g_3(t-t_s) = \omega_p^3\left(-b^3+3b/2\right)\exp\left(-b^2\right), \end{aligned} \tag{13}$$

where $t_s = 1.4/f_p$ is the delay to make the time history causal. It can be shown that the frequency spectrum (time Fourier transform) of these functions is proportional to $\exp\left(f^2/f_p^2\right)$, where $2f_p$ can be considered as a cut-off frequency. The normalization factor 2 on the l.h.s. of (13) is a consequence of Eq. (11).

2.3. Calculation of the Displacements and Accelerations

Each particle velocity component has associated a Green's function G_i, such that

$$v_i = G_i * \dot{h}, \tag{14}$$

where $G_i = \rho^{-1}\partial G/\partial x_i$ because of (1) and (6).

The corresponding displacement component is

$$u_i = \int_0^t v_i dt = G_i * h, \tag{15}$$

i.e., if instead of using g_1 in Eq. (1), we use g_0, we obtain the displacements (see Eq. (13)).

On the other hand, the accelerations are

$$a_i = \dot{v}_i = G_i * \ddot{h}, \tag{16}$$

i.e., if instead of using g_1 in Eq. (1), we use g_2, we obtain the accelerations.

In summary, the choice of the source in Eq. (1) gives

$$\begin{aligned} &\text{Displacements}: \quad \dot{M} = M_0 \delta(x)\,\delta(y)\,\delta(z)\,g_0, \\ &\text{Particle velocities}: \quad \dot{M} = M_0 \delta(x)\,\delta(y)\,\delta(z)\,g_1, \\ &\text{Accelerations}: \quad \dot{M} = M_0 \delta(x)\,\delta(y)\,\delta(z)\,g_2. \end{aligned} \tag{17}$$

Alternatively, the particle velocities and the accelerations can be computed by a numerical differentiation of the displacements and particle velocities, respectively. This approach will be used as a test.

The spatial derivatives are computed by using the Fourier and Chebyshev methods, where the spectral coefficients are calculated with the fast Fourier transform (FFT) (e.g., Carcione *et al.*, 2004). This differential operator is infinitely accurate up to the Nyquist wave number, corresponding to spatial wavelength of two grid points. This means that if the source is band-limited, the algorithm is free of spatial numerical dispersion and aliasing effects, provided that the minimum grid spacing is chosen $dx \leq c_{\min}/(2f_{\max})$, where $f_{\max}$ is the maximum frequency of the source and $c_{\min}$ is the minimum wave velocity.

When solving the velocity-stress formulation with pseudospectral methods, the source can be implemented in one grid point in view of the accuracy of the differential operators. As stated above, the strength of a discrete delta function in the spatial domain is $1/dx$, where dx is the grid size. Since each spatial sample is represented by a cardinal sinc function with argument x/dx (the spatial integration of this function is precisely dx), the introduction of the discrete delta will alias the wavenumbers beyond the Nyquist (π/dx) to the lower wavenumbers. However, if the source time-function $h(t)$ is band-limited with cut-off frequency $f_{\max}$, the wavenumbers greater than $k_{\max} = 2\pi f_{\max}/c_{\min}$ will be filtered. Moreover, since the wave equation is linear, seismograms with different time histories can be implemented by convolving $h(t)$ with only one simulation obtained with $\delta(t)$ as a source, i.e., a discrete delta with strength $1/dt$ [Carcione *et al.*, 2002] (see more details about the modeling algorithm in the appendix).

3. Elastic Wave Equation

The particle velocity-stress formulation for the elastic wave equation is (e.g., Carcione, 2007)

$$\begin{aligned} \dot{v}_1 &= \rho^{-1}(\partial_1\sigma_{11} + \partial_2\sigma_{12} + \partial_3\sigma_{13}), \\ \dot{v}_2 &= \rho^{-1}(\partial_1\sigma_{12} + \partial_2\sigma_{22} + \partial_3\sigma_{23}), \\ \dot{v}_3 &= \rho^{-1}(\partial_1\sigma_{13} + \partial_2\sigma_{23} + \partial_3\sigma_{33}), \\ \dot{\sigma}_{11} &= \bar{\lambda}\theta + 2\bar{\mu}\partial_1 v_1 + \dot{M}_{11}, \\ \dot{\sigma}_{22} &= \bar{\lambda}\theta + 2\bar{\mu}\partial_2 v_2 + \dot{M}_{22}, \\ \dot{\sigma}_{33} &= \bar{\lambda}\theta + 2\bar{\mu}\partial_3 v_3 + \dot{M}_{33}, \\ \dot{\sigma}_{12} &= \bar{\mu}(\partial_1 v_2 + \partial_2 v_1) + \dot{M}_{12}, \\ \dot{\sigma}_{13} &= \bar{\mu}(\partial_1 v_3 + \partial_3 v_1) + \dot{M}_{13}, \end{aligned}$$

$$\dot{\sigma}_{23} = \bar{\mu}(\partial_2 v_3 + \partial_3 v_2) + \dot{M}_{23},$$
$$\theta = \partial_1 v_1 + \partial_2 v_2 + \partial_3 v_3, \tag{18}$$

where σ_{ij} are the stress components, $\bar{\lambda}$ and $\bar{\mu}$ are the Lamé constants and the source terms are

$$M_{ij} = M_0 m_{ij} \delta(x)\, \delta(y)\, \delta(z)\, h(t), \tag{19}$$

where m_{ij} are the moment-tensor components. The moment-tensor formulation [Aki and Richards, 1980] is used to describe the radiation pattern of the source. The Cartesian components are described by the following angles: strike ϕ, dip δ and rake λ. The moment-tensor components are

$$\begin{aligned}
\sqrt{2}m_{11} &= -\left(\sin\delta\cos\lambda\sin 2\phi + \sin 2\delta\sin\lambda\sin^2\phi\right),\\
\sqrt{2}m_{12} &= \left(\sin\delta\cos\lambda\cos 2\phi + \frac{1}{2}\sin 2\delta\sin\lambda\sin 2\phi\right),\\
\sqrt{2}m_{13} &= -(\cos\delta\cos\lambda\cos\phi + \cos 2\delta\sin\lambda\sin\phi),\\
\sqrt{2}m_{22} &= \left(\sin\delta\cos\lambda\sin 2\phi - \sin 2\delta\sin\lambda\cos^2\phi\right),\\
\sqrt{2}m_{23} &= -(\cos\delta\cos\lambda\sin\phi - \cos 2\delta\sin\lambda\cos\phi),\\
\sqrt{2}m_{33} &= \sin 2\delta\sin\lambda,
\end{aligned} \tag{20}$$

such that $m_{ij}m_{ij} = 1$, where implicit summation is assumed. This is the reason for the $\sqrt{2}$ normalization.

Equation (20) is a particular case of a more general moment-tensor formulation describing tensile and shear sources and given, for instance, in Vavryčuk [2011]. The slope angle, φ, describes the tensility of the source, such that $\varphi = 90°$ for pure extensive sources and $\varphi = -90°$ for pure compressive sources. If $\varphi = 0$, we recover the usual moment-tensor components (20) describing shear faulting.

As in the acoustic case, the discrete version is

$$M_{ij} = \frac{M_0}{V} m_{ij} h(t), \tag{21}$$

where V is the volume of the cell, and the time history must satisfy Eq. (11).

4. Examples

4.1. Acoustic Model

The first example considers a homogeneous acoustic medium with $\rho = 2650$ kg/m^3 and $c = 3200$ m/s, and the source time history is $\dot{h} = g_1$(or $h = g_0$), with $f_p = 1$ Hz. The seismic moment is $M_0 = 7 \times 10^{19}$ J (7×10^{26} dyne cm), corresponding to the Messina 1908 earthquake (e.g., Carcione and Kozác, 2008; Carcione and Gei, 2009). The modeling

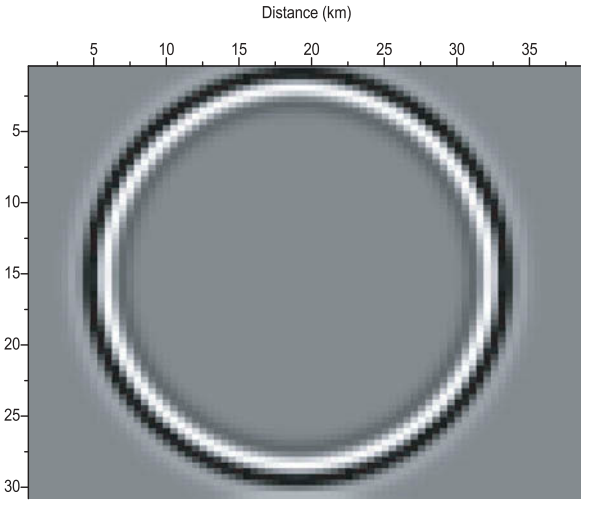

FIGURE 2 Snapshot in the (x, y)-plane of the stress at 6 s.

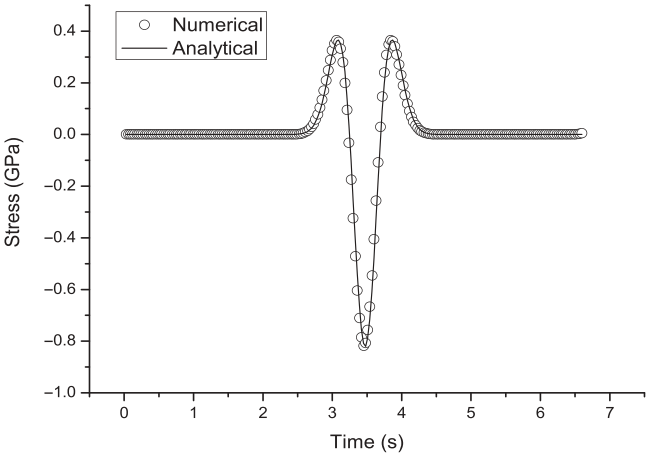

FIGURE 3 Stress. Comparison of numerical and analytical solutions.

algorithm is based on the calculation of the spatial derivatives using the Fourier pseudospectral method along the three spatial coordinates [Carcione, 1993]. The simulations use a $77 \times 77 \times 77$ mesh, with grid spacings $dx = 500$ m, $dy = 400$ m and $dz = 300$ m, and the required time step of the Runge-Kutta algorithm is $dt = 0.03$ s. A snapshot of the stress field at 6 s is shown in Fig. 2. The numerical and analytical solutions are compared in Fig. 3 at (3.5, 3.2, 4.5) km from the source ($r = 6.54$ km). The agreement verifies the correct implementation of the source. Figure 4 shows the particle velocity components.

We now test the calculation of the particle velocity v_1 and acceleration a_1 by two alternative methods. In the first calculation, we use the time history $\dot{h} = g_0$ to obtain the displacement u_1. Then, we compute v_1 by a first-order finite-difference differentiation. This is compared to v_1 obtained by using the source g_1. Figure 5 shows the comparison, where the agreement is excellent. In the second calculation, we use the time history $\dot{h} = g_1$ to obtain the particle velocity v_1. Then, we compute a_1 by a first-order finite-difference differentiation. This is compared to a_1 obtained by using the source g_2. Figure 6 shows the

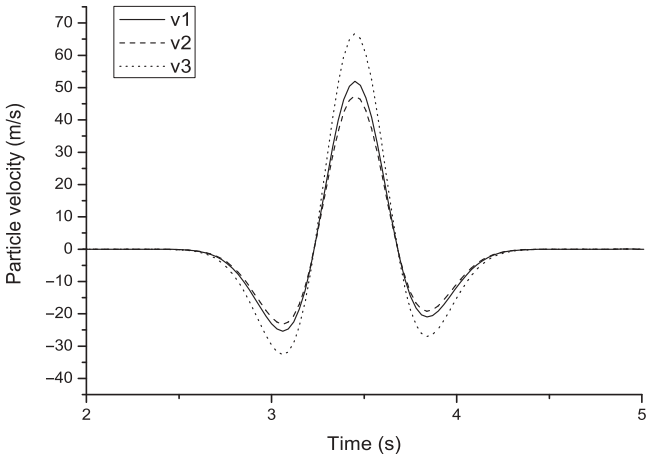

FIGURE 4 Particle velocity components.

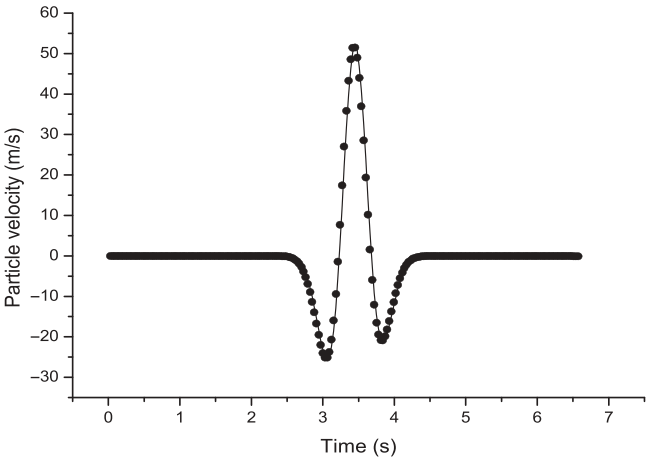

FIGURE 5 Particle velocity component v_1 obtained by two different methods. The solid line corresponds to the source choice given in Eq. (17), while the symbols to a first-order finite difference derivative of the displacement u_1. The L^2-error of the difference between signals is 4×10^{-5}.

comparison. Having tested the approach, we compute the displacements at $r = 6.54$ km, which are shown in Fig. 7.

4.2. Elastic Model

The solution of a similar problem as in Sect. 4.1, but using the elastic equations (18) and the moment tensor (20) is shown in Fig. 8, where $\phi = 20°$, $\delta = 30°$ and $\lambda = 270°$ (e.g., Carcione and Kozác, 2008; Carcione and Gei, 2009) and the medium is a Poisson solid. The difference between Figs. 7 and 8 is the presence of the shear wave in the second simulation after 4 s propagation time.

The preceding examples have not considered a free surface and the spatial derivatives have been computed by using the Fourier pseudospectral method. In the following, we

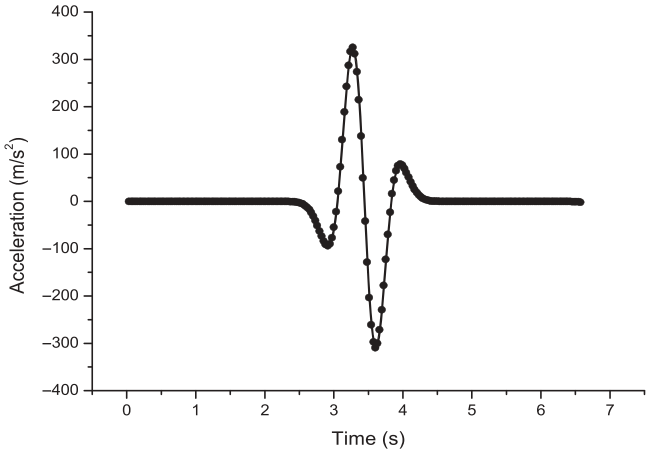

FIGURE 6 Acceleration component a_1 obtained by two different methods. The solid line corresponds to the source choice given in Eq. (17), while the symbols to a first-order finite difference derivative of the particle velocity v_1. The L^2-error of the difference between signals is 3×10^{-6}.

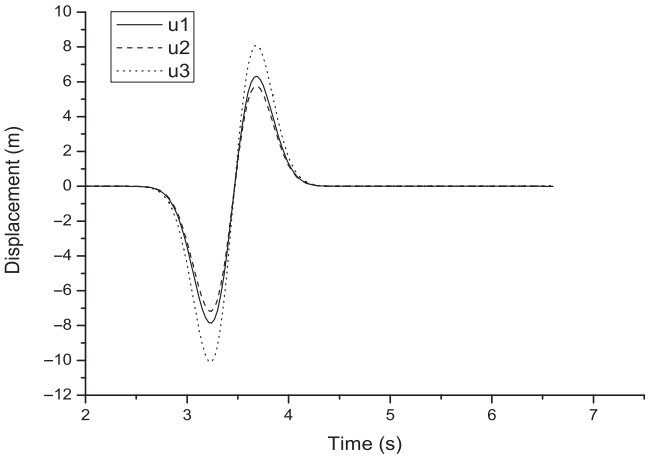

FIGURE 7 Displacement components in the acoustic case.

model the free surface (stress-free condition). In this case, the spatial derivative along the vertical direction is computed with the Chebyshev pseudospectral method [Carcione *et al.*, 2004]. We simulate the propagation from the source DS parameterised by Graves [1996] in his Table 1, where $M_0 = 10^{23}$ dyne cm $= 10^{16}$ J, $\phi = 90°$, $\delta = 90°$ and $\lambda = 90°$ (see his Fig. 5 also). The calculations are based on a homogeneous model, with a P-wave velocity of 4 km/s, an S-wave velocity of 2.3 km/s and a density of 1.8 g/cm^3. The source depth is 2.5 km and the receiver is located at the surface at a horizontal distance of 10 km. The source has a peak frequency $f_p = 1$ Hz. The simulations use a $81 \times 81 \times 81$ mesh, with grid spacings $dx = dy = 500$ m and a vertical extent of 10.45 km. The source is located at the vertical grid point 23, where $dz = 140.5$ m, averaging the adjacent grid sizes, since the grid size is variable along the vertical direction [Carcione *et al.*, 2004]. The time step of the Runge-Kutta algorithm is $dt = 2$ ms. The particle velocity components are shown in Fig. 9,

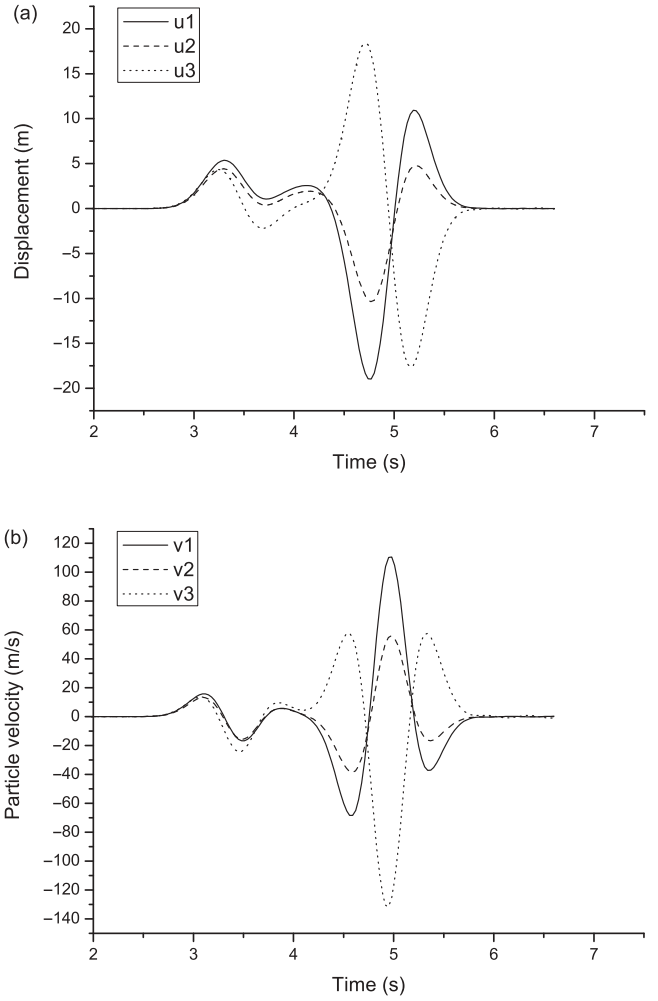

FIGURE 8 Displacement components (a) and particle-velocity components (b) in the elastic case.

where the amplitudes and traveltimes agree with those of Graves [1996] (see his Fig. 5). The horizontal ($y-$) component is zero.

In the case of a spatial distribution of the source, say, involving N grid points, the total moment tensor $M_0 = \sum_{i=1}^{N} M_{0i}$, where M_{0i} is the moment tensor assigned to the i-th grid point. This is due to the linearity of the wave equation.

5. Conclusions

The simulations presented in this work can be used to calibrate the source implementation in direct grid methods, such as finite-difference and finite element algorithms. The result has been tested with the analytical solution in 3D acoustic media. The convolutional Green function form is useful to verify and compute the magnitudes of the displacements, particle velocities and accelerations fields and provide a reliable reference solution. The source implementation holds for any time history other than the Ricker wavelet and in cases where

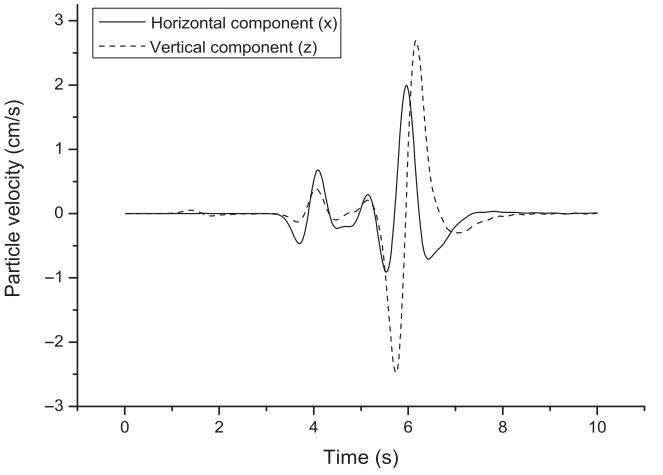

FIGURE 9 Particle-velocity components. The modeling is based on an elastic stress-strain relation and the presence of free surface.

there is seismic anisotropy and attenuation. The method has been shown for a point source, but it can easily be extended to the case of a spatially distributed source.

References

Aki, K., and Richards, P. G. [1980] *Quantitative Seismology: Theory and Methods*, W. H. Freeman and Co, New York.

Carcione, J. M. [1993] "Seismic modeling in viscoelastic media," *Geophysics* **58**, 110–120.

Carcione, J. M. [2007] *Wave Fields in Real Media. Theory and Numerical Simulation of Wave Propagation in Anisotropic, Anelastic, Porous and Electromagnetic Media*, 2nd ed., revised and extended, Elsevier Science, Amsterdam.

Carcione, J. M., and Gei, D. [2009] "Simulation of ground motion and synthetic seismograms. The 1908 Messina Earthquake," *Environmental Semeiotics* **2**(1), 1–15.

Carcione, J. M., Herman, G., and ten Kroode, F. P. E. [2002] "Seismic modeling," *Geophysics* **67**, 1304–1325.

Carcione, J. M., and Kozák, J. [2008] "The Messina-Reggio earthquake of December 28, 1908," *Studia Geophysica et Geodaetica* **52**, 661–672.

Carcione, J. M., Poletto, F., and Gei, D. [2004] "3-D wave simulation in anelastic media using the Kelvin-Voigt constitutive equation," *Journal of Computational Physics* **196**, 282–297.

Dahlen, F. A., and Tromp, J. [1998] *Theoretical Global Seismology*, Princeton University Press, Princeton, NJ

Graves, R. W. [1996] "Simulating seismic wave propagation in 3D elastic media using staggered-grid finite differences," *Bulletin of the Seismological Society of America* **86**, 1091–1106.

Morse P. M., and Feshbach H. [1953] *Methods of Theoretical Physics*, vol. I, McGraw-Hill, New York.

Pitarka, A. [1999] "3-D elastic finite difference modelling of seismic motion using staggered grids with nonuniform spacing," *Bulletin of the Seismological Society of America* **89**, 54–68.

Sheriff, R. E. [2002] *Encyclopedic Dictionary of Exploration Geophysics*, 3rd ed., Society of Exploration Geophysicists, Tulsa, OK.

Tadeu, A. J. B., Santos, P. F. A., and Kausel, E. [1999] "Closed-form integration of singular terms for constant, linear and quadratic boundary elements- Part II: SV-P wave propagation," *Engineering Analysis with Boundary Elements* **23**, 757–768.

Vavryčuk, V. [2011] "Tensile earthquakes: Theory, modeling, and inversion," *Journal of Geophysical Research* B12320, doi:10.1029/2011JB008770.

Appendix: A Modeling Planning

We summarize in the following the steps to perform a simulation with direct grid methods.

1. From the maximum source frequency and minimum velocity, find the constraint on the grid spacing, namely, $dx \leq c_{\min} \big/ (2f_{\max})$. The equality sign implies the maximum allowed spacing to avoid aliasing; that is, two points per wavelength.
2. Find the number of grid points from the size of the model.
3. Allocate additional wavelengths for each absorbing strip at the sides and bottom of the model. For instance, the standard sponge method requires four wavelengths, where the wavelength is $\lambda_d = 2c_{\max} \big/ f_d$ and f_d is the dominant frequency of the seismic signal [Carcione *et al.*, 2002].
4. Choose the time step according to the stability condition and accuracy criteria. For pseudospectral methods a good choice is $dt = 0.2dx \big/ c_{\max}$, where dx is the minimum spacing.
5. Implement the source, using Eq. (10) in the acoustic case and Eq. (20) and (21) in the elastic case. In both cases, the source time history is normalized as in Eq. (11).
6. Locate the receivers in the model, usually at the free surface, and choose the displacement, particle velocity or acceleration fields according to Eq. (17).